

# Self-organized Pattern Formation in Motor-Microtubule Mixtures

Sumithra Sankararaman\* and Gautam I. Menon†

*The Institute of Mathematical Sciences,  
C.I.T. Campus, Taramani,  
Chennai 600 113,  
India.*

P.B. Sunil Kumar‡  
*Department of Physics,  
Indian Institute of Technology Madras,  
Chennai 600 036,  
India.*

(Dated: November 15, 2018)

## Abstract

We propose and study a hydrodynamic model for pattern formation in mixtures of molecular motors and microtubules. The steady state patterns we obtain in different regimes of parameter space include arrangements of vortices and asters separately as well as aster-vortex mixtures and fully disordered states. Such stable steady states are observed in experiments *in vitro*. The sequence of patterns obtained in the experiments can be associated with smooth trajectories in a non-equilibrium phase diagram for our model.

---

\* E-mail : sumithra@imsc.res.in

† E-mail : menon@imsc.res.in

‡ E-mail : sunil@physics.iitm.ac.in

The mitotic spindle is a remarkable self-organized structure formed when a eukaryotic cell divides[1]. It consists of two separated inter-penetrating radial arrays (asters) of long, semi-flexible polymeric filaments with polar character, called microtubules. Molecular motors such as kinesins and dyneins are protein molecules which “walk” unidirectionally along microtubules and exert forces on them, while consuming energy derived from the hydrolysis of ATP. Motor-microtubule interactions play a fundamental role in the formation of the spindle[1].

Interestingly, cell fragments containing both motors and microtubules have been found to exhibit self-organized aster-like structures[2, 3]. Asters and vortices are seen *in vitro*, in experiments on mixtures of molecular motors, microtubules and ATP in a confined quasi-two-dimensional geometry [4, 5]. Studying pattern formation in such simplified contexts may be useful in understanding the vastly more complex problem of spindle formation[6, 7, 8].

These patterns form at large densities of motors and microtubules, rendering first-principles molecular simulations unviable. Such simulations require *ab-initio* modelling of interaction potentials; small errors in these potentials could be amplified at larger scales, thus changing the behavior fundamentally. Further, cellular pattern formation occurs under non-equilibrium conditions. These considerations motivate hydrodynamic approaches in which molecular scale information enters only in terms of coefficients in coarse-grained equations of motion for a few relevant fields[9, 10].

An early attempt at describing such pattern formation is due to Lee and Kardar[11] and motivates the approach described here. Also, detailed Brownian dynamics simulations on a simplified model for motors, microtubules and their interactions have been performed by Nédélec and collaborators, yielding valuable insights[4, 5, 8, 12]. However, these approaches are unsatisfactory in some respects. The Lee-Kardar model fails to reproduce the complex patterns (arrays of asters, vortices and spirals) seen in experiments where the effects of boundaries are minimal. Further, it predicts that the unique steady state at high motor densities should be a single vortex whereas experiments obtain a lattice of asters in this limit[11, 13, 14]. The simulations of Nédélec *et. al.* are computationally intensive, requiring many parameters to be specified[8]. Several of these can be varied substantially without affecting the patterns formed – it is unclear which of them are crucial to pattern formation and which others play a secondary role.

In this Letter, we propose a theory of pattern formation in mixtures of molecular motors

and microtubules. We motivate, using symmetry arguments, hydrodynamic equations of motion for a coarse-grained 2-dimensional vector field ( $\mathbf{T}$ ) representing the local orientation of microtubules as well as for local motor density fields  $m_f$  and  $m_b$  governing densities of “free” and “bound” motors. Motors which move on microtubules are called bound motors, whereas those which diffuse in the solvent are referred to as free motors. Bound and free motors interconvert at rates  $\gamma_{f \rightarrow b}$  and  $\gamma_{b \rightarrow f}$ . Our equations describe the orientation of microtubules by complexes of bound motors, resulting in the formation of patterns at large scales.

Before describing our model we briefly summarize our results: Our model generates virtually all the phases seen in the experiments, including a lattice of asters, a lattice of vortices/spirals[15], a mixture of asters and vortices as well as fully disordered phases[16]. We present a non-equilibrium “phase diagram” for our model; smooth trajectories in this phase diagram can be related to the sequence of states obtained experimentally as the motor density is increased. Such trajectories rationalize the difference in the sequence of patterns formed by different motor species – such as conventional kinesins and NCD’s. We also predict the decay of bound and free motor densities in aster and vortex configurations.

Our equations are derived in the following way: In the absence of interconversion terms changing a bound motor to a free motor,  $m_b$  obeys a continuity equation involving the current of motors transported along the microtubules[11, 14, 17]. The free motor field  $m_f$  obeys a diffusion equation with a diffusion constant  $D$ . These fields are coupled through interconversion terms  $\gamma_{f \rightarrow b}$  (free  $\rightarrow$  bound) and  $\gamma_{b \rightarrow f}$  (bound  $\rightarrow$  free)[17]. We ignore spatial variations in the density of microtubules, concentrating on their orientational degrees of freedom. Our equation for  $\mathbf{T}$  includes terms which reflect the alignment of microtubules by bound motors[11]. We also allow for a motor-independent stiffness against distortions. Finally, and most crucially for our purposes, symmetry permits a term of linear order in gradients of the bound motor density field to appear in the equation of motion for the microtubule field. Putting these ingredients together, we obtain

$$\partial_t m_f = D \nabla^2 m_f - \gamma_{f \rightarrow b} m_f + \gamma_{b \rightarrow f} m_b \quad (1)$$

$$\partial_t m_b = -A \nabla \cdot (m_b \mathbf{T}) + \gamma_{f \rightarrow b} m_f - \gamma_{b \rightarrow f} m_b \quad (2)$$

$$\partial_t \mathbf{T} = \mathbf{T}(\alpha - \beta T^2) + \gamma m_b \nabla^2 \mathbf{T} + \gamma' \nabla m_b \cdot \nabla \mathbf{T} + \kappa \nabla^2 \mathbf{T} + S \nabla m_b \quad (3)$$

The first term in the equation for  $m_b$  describes the motion, with velocity  $A$ , of bound

motors along microtubules. While  $\gamma_{f \rightarrow b}$  should, in principle, depend on the local density of microtubule[14, 17], we argue that such density variations can be *neglected* following coarse-graining to the mesoscopic length-scales of relevance to this problem and at the relatively large concentrations of microtubules in the experiments. We work in two dimensions throughout and scale length in units of  $D/A\sqrt{\beta/\alpha}$ , time in units of  $\beta D/(\alpha A^2)$ , motor densities in units of  $D/\gamma$  and the tubule density in units of  $\sqrt{\alpha/\beta}$ . We choose  $\gamma' = \epsilon\gamma$  and vary the parameter  $\epsilon$ .

The term in  $S$  can be thought of as arising from the variation of a free-energy-like term of the following kind:  $F \sim \int d^2x((\nabla \cdot \mathbf{T}) + Sf(m_b))^2$ . At non-zero  $S$ , such a term clearly favors a spontaneous divergence in the tubule configuration. When motor complexes bind to two parallel tubules, they pull these tubules inwards, generating a wedge-like configuration. Such microscopic dynamics is incorporated in simulations[12] which obtain a lattice of asters. This term arises purely from bound motors and should, for small  $m_b$ , have a strength linear in  $m_b$  *i.e.*  $f(m_b) \sim m_b$ .

Three principal parameters enter our scaled equations:  $\epsilon$ ,  $S$  and the total motor density  $m = m_f + m_b$ . (We take  $\gamma_{f \rightarrow b} = \gamma_{b \rightarrow f} = 0.5$  throughout and choose  $\kappa$  to be 10% of  $m$  so that the motor-induced stiffness is dominant.) We solve the scaled system of equations numerically on an  $L \times L$  square grid[18]. The  $\mathbf{T}$  equation is differenced through the Alternate Direction Implicit (ADI) operator splitting method in the Crank-Nicholson scheme while the equations of motion for the motor density are differenced through an Euler scheme. The grid spacing is  $\delta x = \delta y = \delta = 1.0$ , while the time step is 0.1. We evolve the equations for typically  $2 \times 10^4$  time steps, checking for convergence to steady state. The conservation of total number of motors is imposed by the boundary condition that no motor current flows into or out of the system. We choose “reflecting” boundary conditions for the  $\mathbf{T}$  field, with all tubules at the boundary pointing along the inward normal[19]. We work with systems of several sizes, ranging from  $L = 30$  to  $L = 100$ , varying total motor densities in the range 0.01 to 0.5 in dimensionless units[20].

Figures 1(a) – (d) depict four stable configurations obtained in different regimes of parameter space for an  $L = 100$  lattice. Fig. 1(a) shows a disordered arrangement of microtubules obtained at very low motor densities ( $m = 0.005$ ) with  $\epsilon = 0.5$  and  $S = 0$ . Figure 1(b) shows an aster-vortex mixture obtained at  $m = 0.01$  at the same values of  $\epsilon$  and  $S$ . Note the presence both of well-formed asters and of vortices in the configurations. This figure is

to be contrasted to Fig. 1(c), obtained at  $m = 0.05$ , taking  $\epsilon = 5$  and  $S = 0.001$ . Note the the absence of asters in this regime of parameter space. Finally, Fig 1(d), obtained with  $m = 0.5$ ,  $\epsilon = 1$  and  $S = 1$ , illustrates a lattice of asters phase, with asters being the only stable defects present. We can vary the sizes and numbers of asters obtained in configurations such as the one shown in Fig. 1(d), by changing  $S$ . A larger  $S$  yields a large number of small asters, while smaller values of  $S$  yield a smaller number of large asters[17].

We also predict complex motor density profiles in aster configurations[21]. Our results here differ both from those of Lee and Kardar as well as those of Nédélec, Surrey and Maggs (NSM)[17]. Assuming steady state aster configurations  $\mathbf{T} = -\hat{\mathbf{r}}$  and solving the time-independent equations in steady state yields free motor densities which are a combination of confluent hypergeometric Kummer functions[22]. The bound motor density field satisfies  $\partial_r m_f(r) = -m_b(r)$ . The solution obeys the appropriate boundary conditions (no current at the boundary) and satisfies the normalization constraint on  $m$ . We obtain density profiles for free motors as

$$m_f(r) \sim \frac{e^{-r/\xi}}{r^p} \quad (4)$$

where  $p = \frac{1}{2}(1 - \frac{\gamma_{b \rightarrow f}}{\sqrt{\gamma_{b \rightarrow f}^2 + 4\gamma_{f \rightarrow b}}})$ , and the inverse of the “decay length”  $\xi$  is defined as  $\xi^{-1} = \left| \frac{(\gamma_{b \rightarrow f} - \sqrt{\gamma_{b \rightarrow f}^2 + 4\gamma_{f \rightarrow b}})}{2} \right| = \left| \frac{p\gamma_{b \rightarrow f}}{2p-1} \right|$ . The decay length  $\xi$  and the exponent  $p$  depend on  $\gamma_{f \rightarrow b}$  and  $\gamma_{b \rightarrow f}$ .

Provided  $\xi$  is large compared to the scale of the aster (we estimate  $\xi > 40\mu m$  for typical parameter values), the decay of motor densities is governed principally by the power-law  $m_f \sim 1/r^p$ . With  $\gamma_{f \rightarrow b} = \gamma_{b \rightarrow f} = 0.5$ , we obtain  $p = 1/3$ , although we can generate, as  $\gamma_{f \rightarrow b}$  and  $\gamma_{b \rightarrow f}$  are varied, exponents which vary continuously in the interval  $[0:0.5]$ . (Power-law decays of  $m_f$  are also obtained in the NSM model Ref.[17].)

We relate our scaled parameters to typical experimental values in the following way: The tubule density, scaled in terms of  $\sqrt{\alpha/\beta}$ , is chosen to be unity. The diffusion constant  $D$  is about  $20\mu m^2/s$  and  $A \sim 1\mu m/s$ , defining basic units of length and time as  $20\mu m$  and 20 seconds respectively. A tubule density of 1 implies that over a coarse-graining length of  $400\mu m^2$ , there are around 400 microtubules, a value close to that used in the simulations [5]. The physical length of our simulation box is about  $200\mu m$ , which is in the experimentally relevant regime. Our choice for  $\gamma_{f \rightarrow b}$  and  $\gamma_{b \rightarrow f}$  corresponds to physical rates of  $0.005s^{-1}$  to  $0.05s^{-1}$ , slightly smaller than those in the simulations[8]; using larger rates does not affect

our conclusions here.

Our results are summarized in the qualitative phase diagram of Fig. 2 which shows phases in the three-dimensional space spanned by  $\epsilon$ ,  $S$  and  $m$ . For  $S = 0$ , we obtain a disordered phase at low motor density, which becomes a lattice of vortices at somewhat higher motor densities. Large values of  $\epsilon$  ( $\epsilon \geq 1$ ) yield well-formed vortex-like configurations while small  $\epsilon$  yields structures better described as aster-vortex mixture states. At intermediate values of  $\epsilon$  and  $m$ , spirals rather than vortices appear to dominate. At large  $m$ , with  $S = 0$  and large  $\epsilon$ , a single vortex is obtained[11].

For non-zero but small  $S$ , these phases appear to continue out of the  $S = 0$  plane but are rapidly replaced by a lattice of asters phase for larger  $S$ . A cut of the phase diagram of Fig. 2 at finite  $S$  yields two “phases” - a disordered phase at small  $m$  and a lattice of asters at larger  $m$ . We can thus understand the sequence of patterns formed upon increasing  $m$  in mixtures of kinesin constructs with microtubules in terms of a trajectory which begins in the  $S = 0$  (or  $S$  sufficiently small) plane in the disordered phase and transits between the aster-vortex mixture and lattice of vortices phases (both of which lie in this plane) as  $m$  is increased. As  $m$  increases further and the effects of the  $S$  term become important, such a trajectory moves out towards non-zero  $S$ , encountering the lattice of asters phase.

We have also examined the effects of changing the motor processivity, a quantity proportional to the ratio of  $\gamma_{f \rightarrow b}$  to  $\gamma_{b \rightarrow f}$ . Smaller values of this ratio are appropriate to molecular motors such as NCD. At  $\gamma_{f \rightarrow b} = 0.005$ ,  $\gamma_{b \rightarrow f} = 0.05$ , we find that the disordered regime in the phase diagram of Fig. 2 expands, so that at equivalent values of  $m$  the disordered phase occupies much of the domain associated previously with the lattice of vortices. Whereas kinesins follow the sequence *disordered* – *lattice of vortices* – *aster vortex mixture* – *lattice of asters* as the  $m$  is increased, a mixture of microtubules with NCD motors bypasses the lattice of vortices phase altogether, transiting directly from the disordered phase to the lattice of asters phase in the experiments[5]. In terms of Fig. 2, the expanded regime of disordered phase for the NCD motor suggests that phases such as the lattice of vortices and the aster-vortex mixture may be inaccessible at the motor densities at which the experiments are done, since the effects of the  $S$  term might be expected to dominate at large  $m$ .

In conclusion, we have proposed a hydrodynamic theory capable of generating the sequence of complex phases seen in experiments on pattern formation in mixtures of molecular motors and microtubules and constructed a non-equilibrium phase diagram which contains

these phases. The sequence of phases seen in the experiments on varying motor densities can be reproduced in terms of smooth trajectories in this phase diagram. Our results are also predictive, since we can argue that smooth trajectories in parameter space cannot connect disjoint phases directly. Further details will appear elsewhere[22].

We thank G. Date, J. Samuel, M. Rao and Y. Hatwalne for useful discussions. PBS thanks CSIR, India for support.

- 
- [1] B. Alberts *et. al.* *Molecular Biology of the Cell*, 3<sup>rd</sup> ed. (Garland, New York, 1994).
  - [2] V. Rodionov and G. Borisy, *Nature* **386**, 170 (1997).
  - [3] R. Heald *et. al.* *Jour. Cell Biol.* **138**, 615 (1997); R. Heald *et. al.*, *Nature* **382**, 420 (1996).
  - [4] F. Nédélec *et. al.*, *Nature* **389**, 305 (1997).
  - [5] T. Surrey *et. al.*, *Science* **292**, 1167 (2001).
  - [6] E. Karsenti and I. Vernos, *Science* **294**, 543 (2001).
  - [7] F. Nédélec, T. Surrey and E. Karsenti, *Curr. Opin. Cell Biol.* **23**, 118 (2003).
  - [8] F. Nédélec, *Journal of Cell Biology*, **158**, 1005 (2002).
  - [9] J. Toner and Y. Tu, *Phys. Rev. E* **58**, 4828 (1998).
  - [10] T.B. Liverpool and M.C. Marchetti, *Phys. Rev. Lett*, **90** 138102 (2003).
  - [11] H. Y. Lee and M. Kardar, *Phys. Rev. E* **64**, 056113 (2001).
  - [12] F. Nédélec and T. Surrey, *C. R. Acad. Sci. Paris, Série IV*, 841 (2001).
  - [13] Although we follow earlier authors (see Refs.[4, 5]), in the use of the term “lattice”, we stress that these arrangements are not ordered in any regular manner.
  - [14] J. Kim *et. al.*, *Jour. Kor. Phys. Soc.* **42**, 162 (2003).
  - [15] The experimental patterns seem to resemble spirals more than asters[22].
  - [16] Disordered “bundles” are obtained at still larger  $m$  in the experiments of Ref.[4], but are not reproduced here.
  - [17] F. Nédélec, T. Surrey, A. Maggs, *Phys. Rev. Lett* **86**, 3192 (2001).
  - [18] W. Press *et. al.*, *Numerical Recipes in C*, (Cambridge University Press, Cambridge, 1998).
  - [19] We have checked that the steady state patterns and the structure of our phase diagram remain the same with a variety of different boundary conditions on the  $\mathbf{T}$  field, provided the system size  $L$  is large enough.

- [20] We add weak noise to the tubule equation to ensure that true steady states are reached and have checked, varying both noise and initial conditions, that the patterns we generate are robust.
- [21] Our results for motor density profiles in vortex configurations are the same as those of Ref.[11].
- [22] S. Sankararaman, G.I. Menon and P.B. Sunil Kumar, *in preparation*.



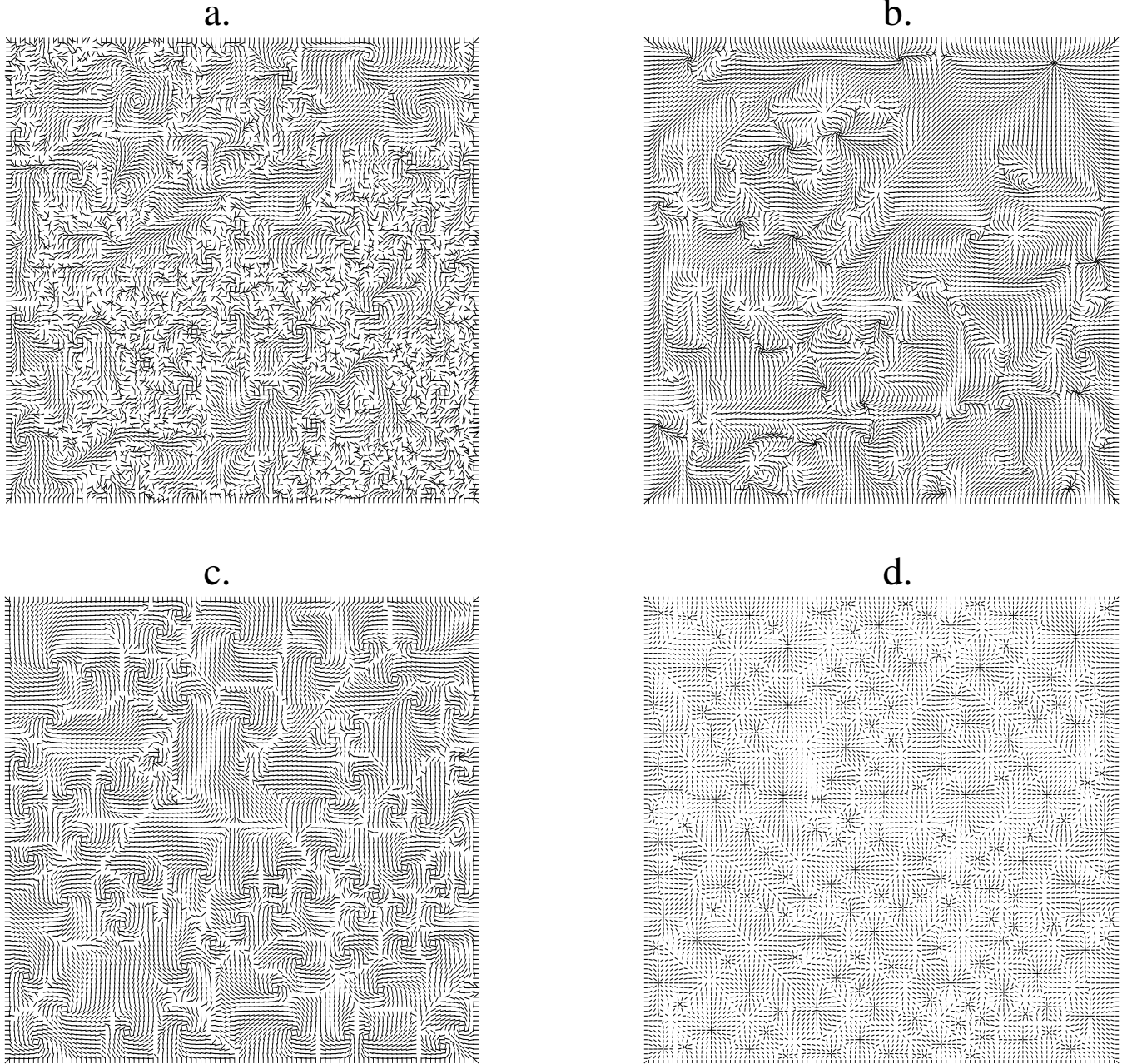


FIG. 1: Steady state configurations in our model at different parameter values (see text): (a) Disordered phase obtained at very low motor densities [ $m = 0.005$ ,  $\epsilon = 0.5$  and  $S = 0$ ]; (b) Aster-vortex mixture obtained at [ $m = 0.01$ ,  $\epsilon = 0.5$  and  $S = 0$ ]; (c) Lattice of vortices at [ $m = 0.05$ ,  $\epsilon = 5$  and  $S = 0.001$ ]; (d) Lattice of asters obtained at [ $m = 0.5$ ,  $\epsilon = 1$  and  $S = 1$ ]

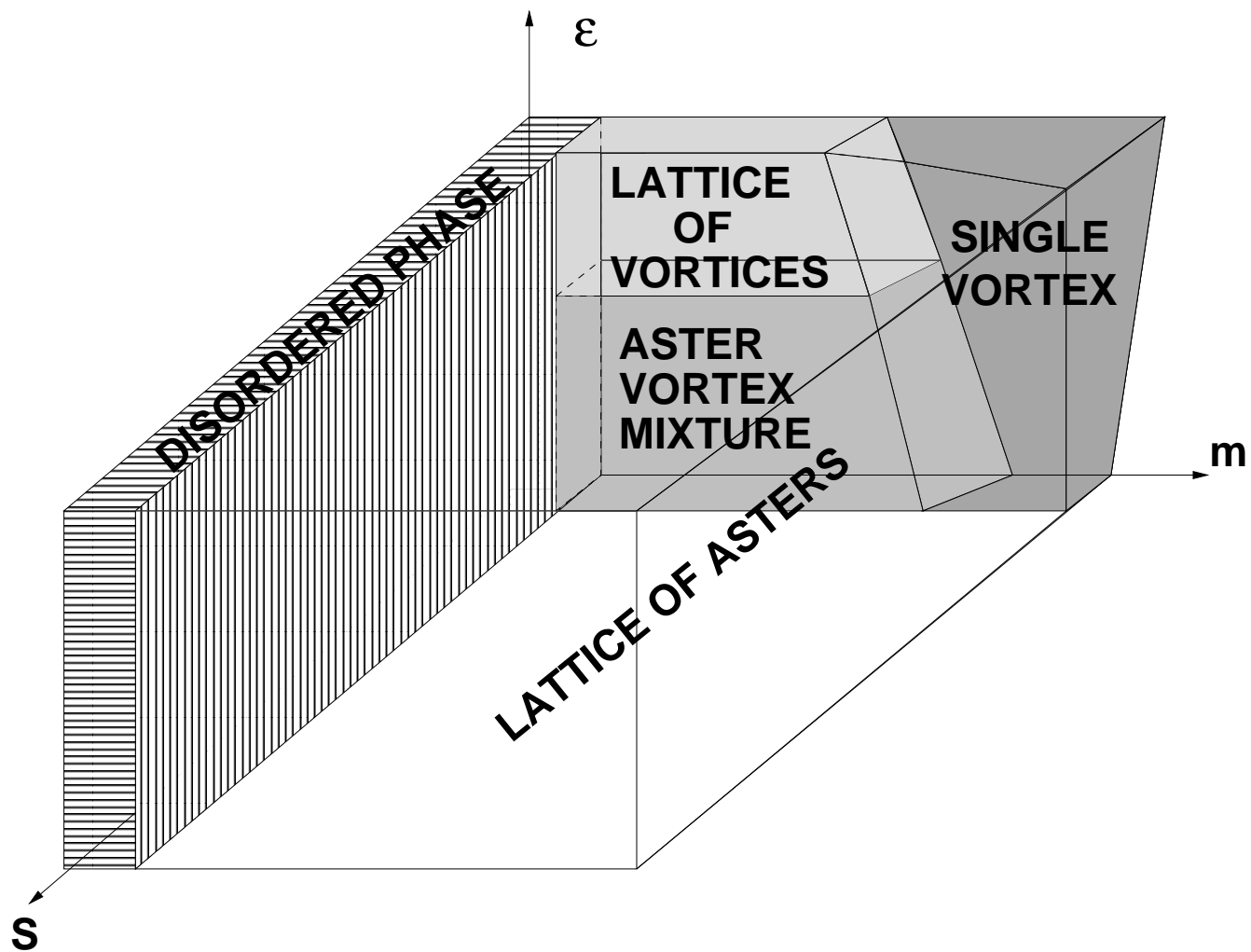


FIG. 2: Schematic phase diagram in the  $\epsilon$ ,  $m$  and  $S$  plane, illustrating the regimes of parameter space in which the phases of Fig. 1 are seen.